FACTA UNIVERSITATIS
Series: **Mechanical Engineering** Vol. 18, Nº 4, 2020, pp. 611 - 621
https://doi.org/10.22190/FUME200520044T

Original scientific paper

INFLUENCE OF TACK WELDS DISTRIBUTION AND WELDING SEQUENCE ON THE ANGULAR DISTORTION OF TIG WELDED JOINT

Jacek Tomków[1], Konrad Sobota[2], Sławomir Krajewski[3]

[1]Gdańsk University of Technology
[2]DAMEN Marine Components
[2]West Pomeranian University of Technology Szczecin

Abstract. *In this paper the influence of tack welds distribution and welding sequence on angular distortion of the Tungsten Inert Gas (TIG) welded joint was tested. Additionally, the effect of welding current on angular distortion was assessed. For research X2CrTiNb18 (AISI 441) stainless steel (2.5 mm thick) was chosen. During research specimens were prepared with different distributions of tack welds. Then they were welded by different welding sequences with the use of different welding current values. After welding the angular distortion of each specimen was measured by using the coordinate measuring machine. In the next step specimens were cut. Cross-sections were polished and the metallographic macroscopic testing was conducted to check the geometry of performed welds. Performed experiments allowed determining the optimal tack weld sequence and welding parameters for welding thin stainless steel sheets*.

Key Words: *Angular Distortion, Tack Welds, TIG Welding, Macroscopic Testing, Weld Geometry, Welding Current*

1. INTRODUCTION

Tungsten Inert Gas (TIG) welding, named also the Gas Tungsten Arc Welding (GTA), is one of the widely used joining processes. It allows for the use of lower heat input values in comparison to other welding methods, which can be helpful in joining thin materials. The process is characterized by high accuracy, which leads to a high quality of welded joints. The method is used for welding alloys of various metals, e.g. nickel [1], aluminum [2], magnesium [3], copper [4], and titanium [5]. It is also widely used in performing dissimilar joints [6-9]. The TIG is also commonly used for joining stainless steels [10,11]. In the case of steel welding, some typical imperfections could be observed. Mahn et al. [12] stated that

Received May 20, 2020 / Accepted October 03, 2020
Corresponding author: Jacek Tomków
Gdańsk University of Technology, Gabriela Narutowicza 11/12 street, 80-233 Gdańsk, Poland
E-mail: jacek,tomkow@pg.edu.pl

TIG welded joints can be characterized by the presence of undercut and burn-through. Fei et al. [13] in their experiment proved that a high welding heat input provides for undercuts in the joint. It has been demonstrated that the welding parameters should be carefully controlled in order to avoid the formation of defects. The other problem during TIG joining is a lack of penetration. The research study of Touilem et al. [14] was focused on elimination of this problem. They observed that weld depth can be increased by welding with the flux activated tungsten inert gas (ATIG) method. Wang et al. [15] proposed novel magnetic arc oscillation as a method allowing us to minimize the number of welding imperfections, and to increase penetration during the TIG welding.

Welding deformations are one of the most important factors affecting the proper production of welding structures. Regardless of the size of the structure, the materials used and the welding method, deformations could always occur [16]. Their causes are the stresses resulting from a welding thermal cycle and a weld shrinkage effect. The thermal cycle depends e.g. on the base metal thickness. Metal sheets with lower thickness are characterized by higher susceptibility to distortion as a result of welding process. Deng and Murakawa [17] presented the thesis that there is almost no temperature gradient through thickness in the thin plate butt joint during welding, which resulted in the formation of distortions in a wide range of welding parameters. Shuaibu Ahmad et al. [18] proved that after the TIG process, welding deformations can be observed. It was also stated that a big deformation induces cracking of the joint.

The welding heat input is an important factor in forming weld deformations. It was stated by Huang et al. [19], that the relationship between heat input and maximum deflection is not linear. There is a critical heat input beyond which the out-of-plane distortion starts to grow very quickly. Qu and Xia [20] carried out a research study on welding numerical simulation. They stated that welding deformations depend on the structures in heat-affected zone (HAZ), which is result of welding heat input. By choosing optimal welding parameters, it is possible to reduce the welding deformations, what was proved by Sudhakaran et al. [21]. One type of the welding deformation is angular distortion. The angular distortion consists of the rotation of the structure around the welding line [22]. The effect of the angular distortion was analyzed by Huang [23]. The experiment showed that the value of this deformation depends on the shielding gas composition. It was also stated that variations in angular distortion are associated with weld depth. Therefore, full penetration welds resulted in lower angular distortion. Tseng and Chou [24] welded austenitic stainless steel with TIG welding process, using a pulsed welding arc. They proved that the angular distortion decreased for materials characterized by higher thermal conductivity.

For experiment ferritic stainless X2CrTiNb18 (AISI 441) steel was chosen. This material is widely used in automotive for parts in the exhaust system, e.g. inlet-/outlet tubes of catalysts and filters [25]. Novel trends showed that high-frequency welding could be used as a joining process for these applications [26,27]. However, the TIG process is most often used. In comparison to austenitic stainless steel, which is widely used in medicine [28], AISI 441 material is characterized by lower plastic strain hardening and the reduced forming limit [29]. X2CrTiNb18 steel presents lower thermal expansion, good oxidation resistance and higher resistance to thermal fatigue [30].

The aim of the research was to study influence of tack welds distribution on the angular distortion of TIG welded joint. The experiments were performed with the use of different welding sequences. Additionally, the influence of different welding current values was

tested. The experiments were prepared to check the possibility of reducing angular distortion after TIG welding of thin ferritic stainless sheets.

2. MATERIALS AND METHODS

2.1. Materials

As a material for experiment, X2CrTiNb18 (AISI 441) steel plates with dimensions of 100×50×2.5 mm were chosen. The structure of base metal (BM) consists of fine-grained ferrite with visible grain boundaries. At the grain boundaries also titanium carbonitride precipitates and very fine niobium carbide separation could be found [31]. The microstructure of used steel is presented in Fig. 1.

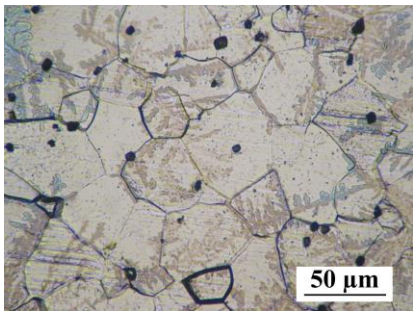

Fig. 1 The microscopic view of X2CrTiNb18 (AISI 441) steel

The chemical composition of used steel has been tested by emission spectroscopy with a spark excitation method with the use of the glow discharge spectrometer LECO GDS 500A (Glow Discharge Atomic Emission Spectrometry). To determine the chemical composition of steel, reference standards for stainless steels were used. The content of elements is presented by mass [%]. As a filler material EN ISO 14343-A:W 19 12 3 L Si rod (1 mm dimension) was selected as a suggested material (by manufacturer) for welding X2CrTiNb18 stainless steel constructions, which will work in chlorides and chlorinated solutions environment. The chemical compositions of used material are listed in Table 1.

Table 1 Chemical composition of used materials, mass %

Material	C	N	Si	Mn	Cr	Nb	S	P	Ti	Other
X2CrTiNb18 (AISI 441) steel	0.023	0.012	0.79	0.95	17.57	0.044	0.002	0.033	0.24	-
EN ISO 14343-A:W 19 12 3 L Si rod in accordance to manufacturer data*	max.0.03	max.0.01	0.80	1.80	19.00	-	-	-	-	Ni – 12.0 Mo – 2.8

2.2. Methods

Welding process was carried out by using manually TIG welding process. For welding WL15 electrode of 1.6 mm diameter was used. The angle of electrode tip was 30°, which provides good penetration during welding of thin sheets. As a shield gas 99.95% argon was used, and the gas flow rate was the 8 l/mm. The post flow value was 10 s. These parameters were chosen in accordance to preliminary investigations. For experiments 21 specimens were performed. They were welded in seventh groups (three specimens in each) with different distribution of tack welds and different welding sequences. The sequence of welding has a significant role in the properties of welded joints, as it affects the residual stresses and welding deformations [32,33]. The welding plan is presented in Table 2. The schematic view of welding procedure is shown in Fig. 2.

Table 2 Specimens welding plan

Group A	Group B	Group C	Group D
five tack welds; progressive welding	five tack welds; step welding (sequence 1)	five tack welds; step welding (sequence 2)	four tack welds; step-back welding
Group E	Group F	Group G	
four tack welds; progressive welding	two tack welds; progressive welding	four tack welds laid outside welding grove; progressive welding	

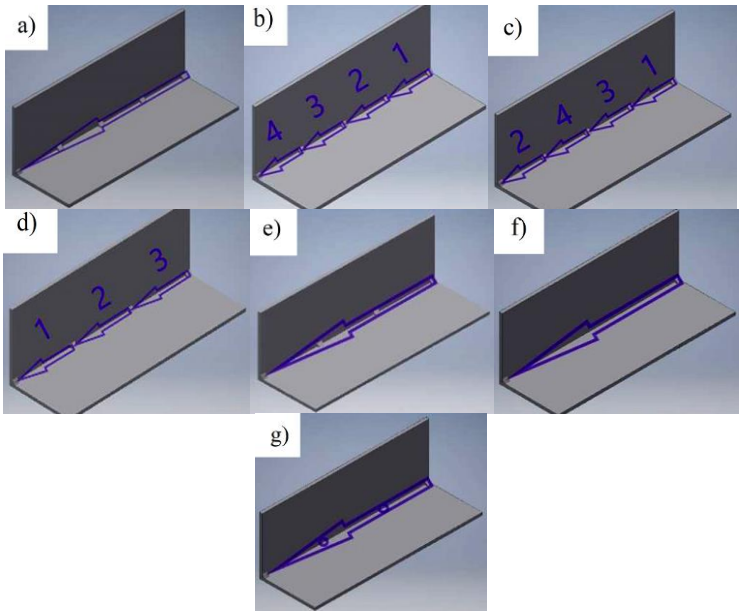

Fig. 2 The schematic view of welding schedule; a) Group A, b) Group B, c) Group C, d) Group D, e) Group E, f) Group F, g) Group G

In each group three specimens have been welded with current (I) values 80 A, 120 A and 160 A. Voltage (U), and welding speed (Vsp) were chosen to provide similar heat input (ql) values in the range 0.20 – 0.25 kJ/mm. The welding speed was calculated after the process, by measuring the welding time and the length of the joint. Before welding sheets were joined by tack welds. Specimens were named by letters A-G which denote a relevant group. The welding parameters of each specimen are listed in Table 3.

Table 3 Welding parameters for prepared specimens

Specimen No	I [A]	U [V]	Vsp [mm/s]	ql [kJ/mm]	Specimen No	I [A]	U [V]	Vsp [mm/s]	ql [kJ/m]
A1	80	10.8	1.62	0.24	E1	80	10.3	2.27	0.22
A2	120	11.2	3.21	0.25	E2	120	11.5	4.05	0.20
A3	160	12.6	4.52	0.21	E3	160	12.4	5.56	0.21
B1	80	10.5	2.19	0.25	F1	80	10.1	2.27	0.21
B2	120	11.7	3.77	0.23	F2	120	11.5	3.85	0.22
B3	160	12.4	5.59	0.25	F3	160	12.5	5.56	0.22
C1	80	10.4	2.34	0.26	G1	80	10.1	2.42	0.20
C2	120	11.2	4.39	0.23	G2	120	12.1	4.31	0.20
C3	160	12.5	5.48	0.25	G3	160	12.3	5.53	0.21
D1	80	10.3	1.90	0.26					
D2	120	11.5	3.13	0.26					
D3	160	12.5	4.55	0.26					

After welding the angular distortion for each specimen was measured by the use of Baty Venture coordinate measuring machine. Test stand was equipped with measuring table, which allows eliminating measurement interference related to drive and environment vibrations. Measurements were taken with the use of 2 mm diameter measurement probe. Specimens with the lowest values of angular distortion were selected for macroscopic testing. Macroscopic tests were performed in accordance with the EN ISO 17639:2013 standard. In each specimen two cross-sections were cut, ground, polished and etched by Vilella's etchant.

3. Results and Discussion

3.1. Angular distortion measurements

Before measurements the measuring table was modified to obtain proper results. The modification consisted in placing stainless steel master plate with threaded holes and specially made blocks, thus enabling quick mounting and facilitating the element's base on the measuring table. Each specimen was divided into sections located every 10 mm (8 sections in specimen). In each section three measurements were done. Each of these three measurement points were determined by the deflection line. Each of the lines was referred to the second sheet plate, which allows accessing the angular distortion of welded joint. The view of measurements results from the Baty Venture coordinate measuring machine is presented in Fig. 3. All of the results are shown in Table 4.

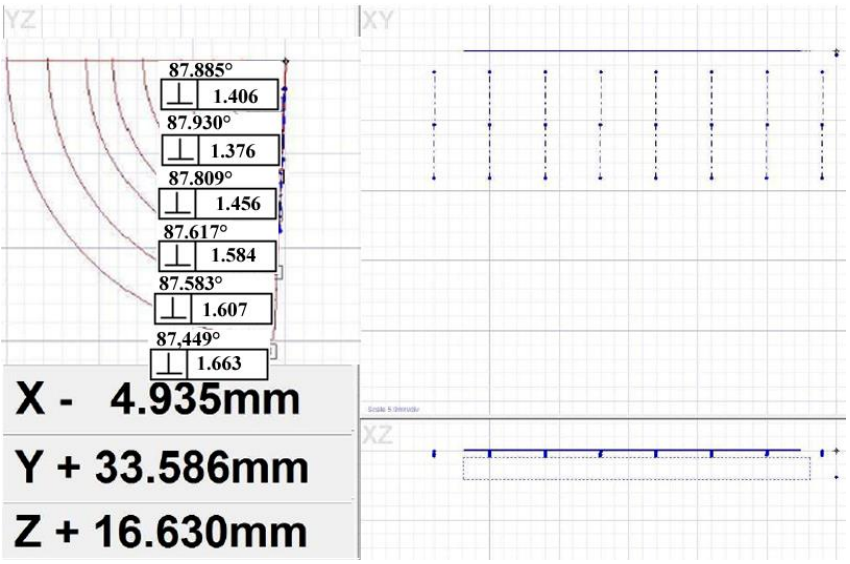

Fig. 3 The view of measurements results by the Baty Venture coordinate measuring machine

Table 4 Results of angular distortion measurements

Specimen No	Avarage angular distortion [°]	Avarage angular distortion in group [°]	Specimen No	Avarage angular distortion [°]	Avarage angular distortion in group [°]
A1	4.12		E1	2.65	2.52
A2	5.63	5.39	E2	2.78	
A3	6.42		E3	2.13	
B1	4.69		F1	1.96	1.38
B2	6.48	5.23	F2	1.14	
B3	4.52		F3	1.03	
C1	3.58		G1	1.61	1.78
C2	3.60	3.99	G2	2.23	
C3	4.79		G3	1.50	
D1	2.48				
D2	1.75	1.86			
D3	1.34				

It was stated in the literature that different welding sequences resulted in different distortion values [34]. This statement was confirmed in the presented study. Chen and Soares [35] performed experiment of thin plates T-joint welding. They stated that short welding passes in one side of the stiffener provide less deformation than a long pass. In this study it is proved that lower angular distortion is an effect of continuous welding with a longer pass (groups F and G). This may be due to the presence of a higher number of tack welds. The highest values of angular distortion were observed for specimens with five tack welds (groups A-C). In the tack welds areas the high stress concentration could be observed. The stresses generate more welding distortion. Similar results were found by

Fu et al. [36]. They stated that progressive welding must be considered firstly in order to avoid the stress concentration at the weld start/end location. The groups A-C were eliminated from further testing.

Okano et al. [37] put forward the thesis that weld distortion is not always precisely evaluated by the weld heat input. It was proved that other factors affecting the weld heat input e.g. welding current should be considered separately. Experiments presented in this paper focused on the angular distortion of TIG filet welded joints. It was proved that, when the welding current increased, the angular distortion decreased. Different results were observed by Narwadkar and Bhosle [38] for MIG welding. It is found that angular distortion is bigger when the current increased but this statement was true for butt-joint. The angular distortion values referred to values of welding current for specimens qualified for further experiments (groups D-G) are shown in Fig. 4.

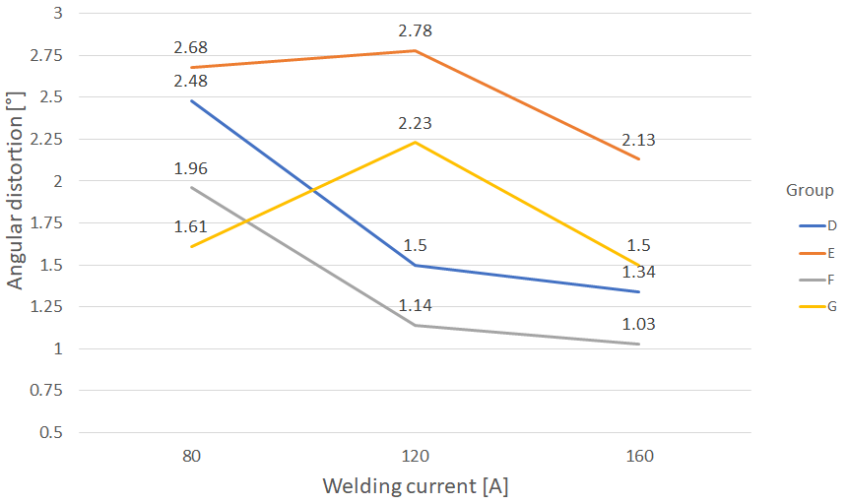

Fig. 4 The angular distortion values referred to values of welding current for specimens qualified to further experiments

3.2. Macroscopic testing

The aim of metallographic macroscopic testing was to check the depth of penetration in each qualified specimen (groups D-H) and measure weld geometry. The methodology of weld geometry measurements is presented in Fig. 5.

The welding parameters were chosen to provide similar values of heat input (0.20 – 0.25 kJ/mm). Preliminary investigations have shown that higher values of heat input affect very high values of angular distortion or provided for melting BM through whole thickness of steel sheet. Due to this fact, increasing the welding current affects increasing the welding speed.

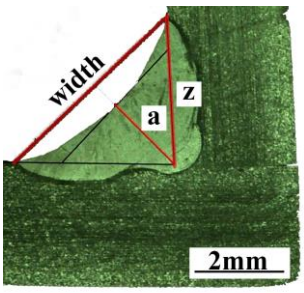

Fig. 5 The methodology of weld geometry measurements

Based on the obtained results the effects of increasing weld width, decreasing penetration in comparison to increasing welding current were observed. Varbai et al. [39] found that a higher welding current provides for increase of the width of weld, which was confirmed in this paper. The effect of welding current on the geometry of performed weld is shown in Fig. 6.

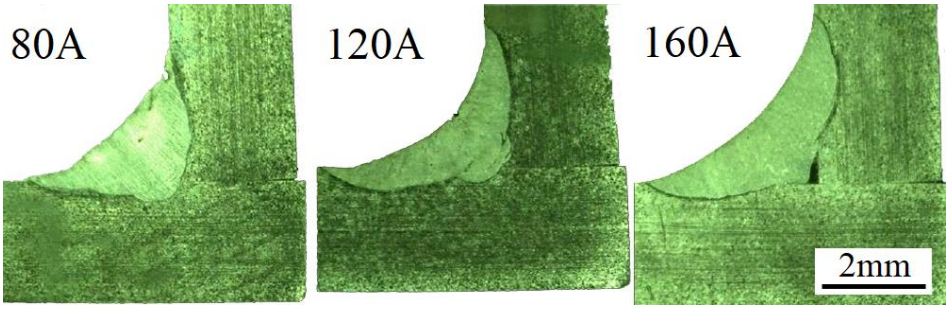

Fig. 6 Effect of welding current on the weld geometry – specimens from group E

Additionally, the lack of penetration was found in the specimens welded with the current equal to 160 A (Fig. 6b and Fig. 6c), which were welded with a smaller welding speed. One way of increasing the depth of weld is by decreasing the welding speed. However, the welding with smaller welding speed did not allow for forming a proper welded joint. Varbai et al. [40] found that the thermal cycle has a significant role in formation structures in HAZ, which may cause deformations. Due to this statement, a lower welding speed may decrease the value of angular distortion. However, during preliminary investigations it was observed that lower welding speed also caused high numbers of undercuts. The results of macroscopic tests are presented in Fig. 7. The results of geometry measurements are listed in Table 5.

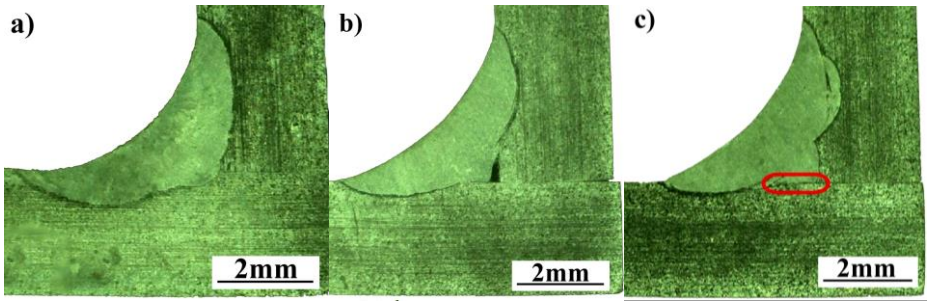

Fig. 7 Results of macroscopic tests; a) specimen D2, b) specimen E3, c) specimen G3, lack of fusion mark by red ellipse

Table 5 Results of geometry measurements

Specimen No	width [mm]	a [mm]	z [mm]	Penetration
D1	3.49	2.33	1.62	+
D2	4.23	3.25	1.65	+
D3	4.49	3.07	1.68	–
E1	3.80	3.21	1.7	+
E2	4.27	3.13	1.38	+
E3	4.70	3.46	1.66	–
F1	3.46	2.44	1.77	+
F2	4.46	3.01	1.59	+
F3	4.65	3.33	1.72	–
G1	3.66	3.24	1.78	+
G2	4.22	3.21	1.65	+
G3	4.82	3.57	1.78	-

5. CONCLUSIONS

In the paper the effects of tack weld distribution and welding sequence on the angular distortion were investigated. Additionally, the influence of welding current was assessed. Performed experiments showed that all of investigated factors have a significant impact on the angular distortion of TIG welded fillet joints. It was proved that an increasing number of tack welds affect increasing angular distortion. Also, the step welding technique provides for the increase of the mentioned type of distortion. Additionally, it was found that welding with a higher value of welding current leads to the decrease of the angular distortion. However, it also caused lack of penetration. The main conclusions resulting from experiments are:

1. The number of tack welds has a significant impact on the angular distortion of X2CrTiNb18 (AISI 441) steel filet welded joints. It was proved that an increasing number of tack welds provides for higher values of angular distortion. The lowest values of distortion (1.03° and 1.14°) were observed for specimens from group G, in which two tack welds were laid before test welding.
2. The angular distortion of welded joints made of stainless steel can be changed with different welding techniques. During welding of thick TIG welded joints the progressive technique provides for lower values of angular distortion, which was observed for specimens from groups F and G.
3. Increasing welding current from 80 to 160 A caused decreasing angular distortion of the performed joints. This effect was observed for each of the tested group. For experiments, specimens welded with different welding current (80 A, 120 A and 160 A) were performed. Other parameters were chosen to provide for heat input values in the range 0.20 – 0.25 kJ/mm, which allow minimizing the influence of the effect of the heat input on the angular distortion. However, increasing of the welding current caused an increasing welding speed, which resulted in the lack of penetration in specimens welded with 160 A.
4. As referenced parameters for X2CrTiNb18 (AISI 441) stainless steel filet welded joints, the parameters shown in this paper should be used. It allows avoiding

occurring welding imperfections, and minimizing the angular distortion of the performed joints. For welding progressive technique should be used. Also, if it is possible, the tack welds should be laid outside the welding groove. If it is not possible, the number of tack welds should be reduced to two.

REFERENCES

1. Park, J.H., Cheeou, M., Cho, S.M., 2020, *Analysis and characterization of the weld pood and bead geometry of inconel 625 Super-TIG welds*, Metals, 10(3), 365.
2. Cai, X., Lin, S., Wang, X., Yang, C., Fan, C., 2019, *Characteristics of periodic ultrasonic assisted TIG welding for 2219 aluminum alloys*, Materials, 12(24), 4081.
3. Song, G., Diao, Z., Lv, X., Liu, L., 2018, *TIG and laser-TIG hybrid filler wire welding of casting and wrought dissimilar magnesium* alloy, Journal of Manufacturing Processes, 34(part A), pp. 204-214.
4. Cheng, Z., Huang, J., Ye, Z., Chen, Y., Yang, J., Chen, S., 2019, *Microstructures and mechanical properties of copper-stainless steel butt-welded joints by MIG-TIG double-sided arc welding*, Journal of Materials Processing Technology, 265, pp. 87-98.
5. Górka, J., Przybyła, M., Szmul, M., Chudzio, A., Ładak, D., 2019, *Orbital TIG welding of titanium tubes with perforated bottom made of titanium-clad steel*, Advances in Materials Science, 19(3), pp. 55-64.
6. Sharma, P., Dwivedi, D.K., 2019, *A-TIG welding of dissimilar P92 steel and 304H austenitic stainless steel: Mechanisms, microstructure and mechanical properties*, Journal of Manufacturing Processes, 44, pp. 166-178.
7. Fei, Z., Pan, Z., Cuiuri, D., Li, H., Van Duin, S., Yu, Z., 2019, *Microstructural characterization and mechanical properties of K-TIG welded SAD2205/AISI316L dissimilar joint*, Journal of Manufacturing Processes, 45, pp. 340-355.
8. Karthi, S., Kumaresh Babu, S.P., Shanmugham, S., Balaji, V.P., 2019, *Study on the dissimilar joining of martensitic stainless steel and carbon steel using TIG welding*, Advances in Additive Manufacturing and Joining, pp. 545-554.
9. Rogalski, G., Fydrych, D., Landowski, M., Świerczyńska, A., 2020, *Mechanical and microstructural characterization of TIG welded dissimilar joints between 304L austenitic stainless steel and Incoloy 800HT nickel alloy*, Metals, 10(5), 449.
10. Garg, H., Sehgal, K., Lamba, R., Kajal, G., 2019, *A systematic review: Effect of TIG and A-TIG welding on austenitic stainless steel*, Advances in Industrial and Production Engineering, pp. 375-385.
11. Feng, C., Qin, G., Meng, X., Peihao, G., 2020, *Defect evolution of 409L stainless steel in high-speed TIG welding*, Materials and Manufacturing Processes, 35(2), pp. 179-186.
12. Manh, N.H., Anh, N.V., Tuan, N.V., Xu, B., Akihisa, M., 2019, *Research and development of novel TIG welding torch for joining thin sheets*, Applied Sciences, 9, 5260.
13. Fei, Z., Pan, Z., Cuiuri, D., Li, H., Wu, B., Ding, D., Su, L., 2019, *Effect of heat input on weld formation and tensile properties in keyhole mode TIG welding process*, Metals, 9, 1327.
14. Touilem, K., Ouis, A., Djoudjou R., Chihaoui Hedhibi, A., Alrebei, H., Albaijan, I., Alzahrani, B., Sherig, E-S.M., Abdo, H.S., 2020, *Effects of ATIG welding on weld shape, mechanical properties, and corrosion resistance of 430 ferritic stainless steel alloy*, Metals, 10, 404.
15. Wang, J., Sun, Q., Feng, J., Wang, S., Ahao, H., 2017, *Characteristics of welding and arc pressure in TIG narrow gap welding using novel magnetic arc oscillation*, The International Journal of Advanced Manufacturing Technology, 90, pp. 413-420.
16. Zavdoveev, A., Rogante, M., Heaton, M., Acquier, P., Kim, H.S., Baudin, T., Kostin, V., 2020, *Development of the PC-GMAW welding technology for TMCP steel in accordance with welding thermal cycle, welding technique, structure, and properties of welded joints*, Reports in Mechanical Engineering, 1(1), pp. 26-33.
17. Deng, D., Murakawa, H., 2007, *Prediction of welding distortion and residual stress in a thin plate butt-welded joint*, Computational Materials Science, 42(2), pp. 353-365.
18. Shuaibu Ahmad, A., Wu, Y., Gong, H., Nie, L., 2019, *Finite element prediction of residual stress and deformation inducted by double-pass TIG welding of Al 2219 plate*, Materials, 12, 2251.
19. Huang, H., Yin, X., Feng, Z., Ma, N., 2019, *Finite element analysis and in-situ measurements of out-of-plane distortion in thin plate TIG welding*, Materials, 12, 141.
20. Qu, Z., Xia, L., 2019, *Study on welding numerical simulation for ultra-high strength steel BS690E*, Procedia Manufacturing, 37, pp. 97-104.

21. Sudhakaran, R., Vel Murugan, V., Sivasakthivel, P.S., 2012, *Optimization of process parameters to minimize angular distortion in gas tungsten arc welded stainless steel 202 grade plates using particle swarm optimization*, Journal of Engineering Science and Technology, 7(2), pp. 195-209.
22. Adamczuk, P.C., Machado, I.G., Mazzaferro, J.A.E., 2017, *Methodology for predicting the angular distortion in multi-pass butt-joint welding*, Journal of Materials Processing Technology, 240, pp 305-313.
23. Huang, H-Y., 2009, *Effect of shielding gas composition and activating flux on GTAW weldments*, Materials & Design, 30(7), pp. 2404-2409.
24. Tseng, K.H., Chou, C.P., 2013, *Effect of pulsed gas tungsten arc welding on angular distortion in austenitic stainless steel weldment*, Science and Technology of Welding and Joining, 6(3), pp. 149-153.
25. Reuther, A., Mosel, A., Freytag, P., Lambarri, J., Degenkolb, L., Werner, M., Winter, S., 2019, *Numerical and experimental investigations for hot metal gas forming of stainless steel X2CrTiNb18*, Procedia Manufacturing, 27, pp. 112-117.
26. Li, J., Sun, Q., Liu, Y., Zhen, Z., Sun, Q., Feng, J., 2020, *Melt flow and microstructural characteristics in beam oscillation superimposed laser welding of 304 stainless steel*, Journal of Manufacturing Processes, 50, pp. 629-637.
27. Kang, K., Liu, Y., Li, J., Liu, C., Zhen, Z., Wang, Y., Sun, Q., 2020, *Microstructure and mechanical properties of Al/steel butt joint by hybrid CMT welding with external axial magnetic field*, Materials, 13(16), 3601.
28. Singh, G., Lamichhane, Y., Bhui, A.S., Sidhu, S.S., Bains, P.S., Mukhiya, P., 2019, *Surface morphology and microhardness behavior of 316L in HAP-PMEDM*, Facta Universitatis-Series Mechanical Engineering, 17(3), pp. 445-454.
29. Charles, J., Mithieux, J.D., Santacreu, P.O., Peguet, L., 2009, *The ferritic stainless steel family: The appropriate answer to nickel volatility?*, Revue de Métallurgie – International Journal of Metallurgy, 106(3), pp. 124-139.
30. Ikea, K., Yamoah, N.K.G., Reynolds, W.T., Hamada, J., Murayama, M., 2015, *Effect of laves phase on high-temperature deformation and microstructure evolution in an 18Cr-2Mo-0.5Nb ferritic stainless steel*, Journal of Metallurgical and Materials Transactions A, 46(8), pp. 3460-3469.
31. Żuk, M., Czupryński, A., Czarnecki, D., Poloczek, T., 2019, *The effect of niobium and titanium in base metal and filler metal on intergranular corrosion of stainless steels*, Welding Technology Review, 91(6), pp. 30-38.
32. Tomków, J., Fydrych, D., Rogalski, G., 2019, *Role of bead sequence in underwater welding*, Materials, 12, 3372.
33. Tomków, J., Janeczek, A., 2020, *Underwater in situ local heat treatment by additional stitches for improving the weldability of steel*, Applied Sciences, 10(5), 1823.
34. Gannon, L., Liu, Y., Pegg, N., Smith, M., 2010, *Effect of welding sequence on residual stress and distortion in flat-bar stiffened plates*, Marine Structures, 23(3), pp. 385-404.
35. Chen, B-Q., Soares, C.G., 2016, *Effects of welding sequence on the temperature distribution, distortions, and residual stress on stiffened plates*, International Journal of Advanced Manufacturing Technology, 86, pp. 3145-3156.
36. Fu, G., Lourenço, M.I., Duan, M., Estefan, S.F., 2015, *Influence of the welding sequence on residual stress and distortion of fillet welded structures*, Marine Structures, 46, pp. 30-55.
37. Okano, S., Mochizuki, M., Yamamoto, K., Tanaka, M., 2011, *An attempt to enhance numerical models of angular distortion by considering the physics of the welding arc*, Welding in the World, 55, pp. 93-100.
38. Narwadkar, A., Bhosle, S., 2016, *Optimization of MIG welding parameters to control the angular distortion in Fe410WA steel*, Materials and Manufacturing Processes, 31(16), pp. 2158-2164.
39. Varbai, B., Adonyi, Y., Baumer, R., Pickle, T., Dobránszky, J., Májlinger, K., 2019, *Weldability of duplex stainless steels – thermal cycle and nitrogen effects*, Welding Journal, 98, pp. 78-87.
40. Varbai, B., Pickle, T., Májlinger, K., 2019, *Effect of heat input and role of nitrogen on the phase evolution of 2205 duplex stainless steel weldment*, International Journal of Pressure Vessels and Piping,176, 103952.